Journal of *Marine Science and Engineering*

MDPI

Article

Fishing Vessel Bulbous Bow Hydrodynamics—A Numerical Reverse Design Approach

Héctor Rubén Díaz Ojeda [1,*], Sebastian Oyuela [2], Roberto Sosa [3], Alejandro Daniel Otero [4] and Francisco Pérez Arribas [5,*]

[1] Instituto Universitario de Sistemas Inteligentes y Aplicaciones Numéricas en Ingeniería, Universidad de Las Palmas de Gran Canaria, 35017 Las Palmas, Spain
[2] Canal de Experiencias de Arquitectura Naval (CEAN), Facultad de Ingeniería, Universidad de Buenos Aires, Buenos Aires C1063, Argentina; soyuela@fi.uba.ar
[3] Canal de Experiencias de Arquitectura Naval (CEAN), Instituto de Tecnologías y Ciencias de la Ingeniería "Hilario Fernández Long" (INTECIN), Buenos Aires C1063, Argentina; rsosa@fi.uba.ar
[4] Centro de Simulación Computacional para Aplicaciones Tecnológicas (CSC), Consejo Nacional de Investigaciones Científicas y Técnicas (CONICET), Buenos Aires C1425, Argentina; aotero@fi.uba.ar
[5] Departamento Arquitectura Construcción y Sistemas Oceánicos y Navales, Universidad Politécnica de Madrid, Calle Ramiro de Maeztu, 7, 28040 Madrid, Spain
* Correspondence: hectorruben.diaz@ulpgc.es (H.R.D.O.); francisco.perez.arribas@upm.es (F.P.A.)

Abstract: Naval hydrodynamics typically focus on reducing ship resistance, which can be achieved by incorporating a bulbous bow. This feature is commonly used in the merchant fleet and smaller vessels, such as fishing boats, to minimize wave-making resistance. However, it is important to note that the use of a bulbous bow may not always be necessary or effective in all ship designs. In some cases, fishing ship designs may include a bulbous bow that is not optimized due to the use of procedures and methods intended for larger merchant ships or based on past experience. This study examines the effect of different bow designs, including the bulbous bow, on ship resistance in calm water, with a focus on a typical Argentinian trawler fishing vessel. The objective of this research is to assess the hydrodynamics of various designs for a particular ship by modifying its vessel lines. Firstly, the bulbous bow is removed, and then the reduction in ship resistance achieved by the bulbous bow under different load conditions and speeds is evaluated by comparing the vessel with and without the bulbous bow. The numerical analysis is performed using OpenFOAM, and the results are validated through towing tank experiments. This research indicates that the performance of the bulbous bow varies under different conditions. Therefore, it is recommended to conduct an initial study and a full evaluation of the design and operation alternatives.

Keywords: ship resistance; EFD and CFD; fishing vessels; bulbous bow; ship design

Citation: Díaz Ojeda, H.R.; Oyuela, S.; Sosa, R.; Otero, A.D.; Pérez Arribas, F. Fishing Vessel Bulbous Bow Hydrodynamics—A Numerical Reverse Design Approach. *J. Mar. Sci. Eng.* **2024**, *12*, 436. https://doi.org/10.3390/jmse12030436

Academic Editors: Abdellatif Ouahsine and Peng Du

Received: 23 January 2024
Revised: 26 February 2024
Accepted: 27 February 2024
Published: 29 February 2024

1. Introduction

In naval hydrodynamics, one of the main evaluations that should be carried out in the early stages of ship design is the ship's resistance. This is related to the operational speed of the ship that is established in the ship's contract. An accurate prediction is basic for an appropriate ship use. In addition, this resistance will influence other areas such as engine selection, stability analysis, scantling, etc., without taking into account the huge impact that might be produced on the ship's operation, profitability, and performance.

Historically, when dealing with the early stages of ship design, nonexpensive and accessible procedures are used. These procedures are regression and statistical methods based on database information from previous towing tank experiments and sea trials, such as [1] or, one of the most used, the Holtrop and Mennen method [2]. These methods are used as guides, but they are also used with certain caution due to the uncertainties presented when compared with numerical or experimental studies, such as those presented

by [3], where discrepancies of up to 30% in ship resistance were found for fishing vessels. In [4], there are also large differences in resistance found between regression methods and CFD. As it was presented, these differences present a high impact on environmental inefficiencies which might lead to a wrong design or even operational problems. The presented differences come, for instance, from the fact that regression and statistical methods are unable to evaluate the skills of a naval architect drawing lines or drawing a bulbous bow in different ways.

As the design stages progress, the needs change towards more reliable and accurate methods or procedures. These methods are required since a good capture of the drawing lines effects, viscous effects, or wave breaking, among others, is essential for a good resistance evaluation. Nowadays, two procedures are the most used and recognized by the ITTC (International Towing Tank Conference). On the one hand, experimental fluid dynamic (EFD) tests carried out in towing tanks are considered the most reliable procedure. On the other hand, there are computational fluid dynamics (CFD) simulations that allow many different trials and visualizations for those that do not have access to experimental results as a reliable alternative, as is presented in the text of [5]. This last alternative is commonly used in design as a tool for testing different design concepts during the last years, commonly validated and used for ship resistance determination in calm water.

For the research community and experts in the field, the ITTC publishes Recommended Procedures in order to establish guidelines to follow for a consistent methodology both numerical and experimental in order to obtain the most accurate and reproducible results with a minimum error.

In hull design, a bulbous bow is commonly incorporated below the waterline because it helps reduce total drag and installed power, improving the economics of the design by reducing fuel consumption. Assuming the vessel maintains a consistent speed, an appropriate bulbous bow design can lead to favorable interference between the bow waves generated by the bulb and those generated by the hull alone. According to [6,7], this can lead to a decrease in resistance of between 12% and 15%. Other types of bows, such as dihedral bulbous bows, have been confirmed in [8,9] as good alternatives for ship resistance. These bulbous bows present a resistance reduction for small fishing vessels under varying loads and speeds. The study was performed with model scale ships and calm water, numerically and experimentally noting that the use of a bulbous bow should be considered once a certain speed is reached.

However, an erroneous design may cause a detrimental interaction between these two wave systems, resulting in a substantial rise in ship resistance. This topic, for instance, is important, as shown in [10]. Due to the complex interactions between the bulbous bow waves and hull, ship designs cannot be universally efficient or standardized for all speeds and operating conditions. This is because different speeds and varying load conditions must be taken into consideration for each vessel's operation. When traveling to and from fishing grounds, trawler fishing vessels experience different displacements and speeds. It is important to note that the weight of the fish capture can also impact the displacement and speed of the vessel when returning to port. These can also be affected by factors such as weather conditions and competition with other fishing vessels. In this sense, the bulbous bow is placed in a fixed ship, which makes the ship have different efficiencies according to the specific operation condition that the ship has throughout its lifetime. For this reason, sometimes, the election of a bulbous bow is mostly a compromise election that is based on multiple considerations and evaluations.

Designing a bulbous bow is a complex and controversial task that lacks a standardized procedure. Model tests have been conducted to select an optimal bulbous bow design with minimal resistance, but they can be time-consuming and expensive [11]. Numerical methods can aid the design process when model tests are not feasible. The authors of [12] conducted one of the most well-known experimental studies on bulbous bow models. The study involved testing numerous models and using statistical analysis to develop design charts that are commonly used in bulbous bow design. The study involved testing

numerous models and using statistical analysis to develop design tables that are commonly used in bow design, but the tables are not suitable for smaller fishing vessels, and if used by design engineers, the resultant bow may not be optimal due to the differences between the designed bow and those used in the trials designed for larger vessels.

Previous research is based on Kracht's work [13] or [14]. Some studies use CFD analysis to optimize design variables, such as the length, breadth, frontal area, and depth of a bulbous bow. CFD has been used more often than experimental studies [15–17].

Bulbous bows have been applied in Argentinian fishing vessels. In Argentina, the fishing industry has changed since 1960. Hake fishery started in 1961, changing into the incorporation of fresh fish ships in 1970, which brought an enhancement of the capture quality and freshness. In 1976, processing ships allowing freezing were introduced, while in the 1980s, an expansion of the shrimp fishery appeared [18]. Nowadays, Argentina has started a fleet modernization using more environmentally sustainable technologies to improve crew safety. Aligning with this modernization, studies of hydrodynamic optimizations might be interesting from a consumption and operation point of view, with whether to use or not use a bulbous bow being one of the most relevant topics.

This study aims to assess the effectiveness of a bulbous bow for a fishing trawler that has been in use for over 20 years. This research began with the design and validation approximation presented in [19,20]. The ship lines used are the typical lines of an Argentinian fishing vessel which was initially designed with a bulbous bow. To achieve this, the authors decided first to evaluate the hydrodynamics of the original vessel with a bulbous bow numerically and experimentally in order to quantify its resistance and hydrodynamic behavior. The plan was to remove the bulbous bow from the original ship design, which is a unique and innovative approach to ship design. This inverse procedure has no previous references. Using CFD, this study compares the hydrodynamic behavior of the original hull with the bulbous bow with the two hulls designed without it. The results provide valuable insights into the range of applications of the original bulbous bow and two typical fishing bow designs. This will lay the foundation for future bow designs using the knowledge gained from these studies. This research provides valuable data for different operational conditions of a fishing vessel and also provides useful information on bow behavior in calm water that can be used for consideration in different cases. The results are in a field where limited research is found, which makes it important to evaluate the forces' decomposition for each case that identify the determinant factors for each case of sailing, because this will provide some useful ideas for naval designers when this topic is considered.

This paper is organized as follows: A description of the model and full-scale ship, the towing tank, and the experimental setup is presented in Section 2. The numerical set-up and procedure are described in Section 3. The results are presented in Section 4, and finally, the main conclusions are given in Section 5.

2. Towing Tank Experiments

Towing tank experiments are the traditional way of obtaining the resistance–velocity curve for a specific ship. The accuracy provided by the experiments allows one to validate the numerical procedure with the obtained results. For this reason, in this work, the total model resistance is measured by Froude numbers (Fn) between 0.1 and 0.45. With Fn defined as

$$\mathrm{Fn} = \frac{V}{\sqrt{gL_{WL}}} \tag{1}$$

with V being the model ship velocity, L_{WL} the model length on the waterline, and g the acceleration of gravity. As mentioned in the introduction, towing tank experiments are highly costly. For that reason, it was decided to only experimentally study the original case, the ship with a bulbous bow, which will serve as the CFD validation.

2.1. Model Ship Description

In the present research, the ship lines used are similar to a typical Argentine fishing vessel. This ship is built with a model scale λ = 20 using Glass-Fiber Reinforced Plastic (GFRP), taking into account the ITTC procedures for manufacturing [21]. Special attention was paid to tolerances and surface finish manufacture, as well as the location and size of the turbulence stimulation wires.

The principal characteristics of the model and full-scale ship are presented in Table 1. This table represents the case with a bow of a typical Argentinian fishing vessel. Three load conditions (LC) are presented in Table 1 for the model scale, since a full evaluation of those three load conditions will be performed. These are identified as a full load condition (LC heavy), an intermediate load condition (LC medium), and a ballast condition (LC light). The principal characteristics of the full-scale ship are presented only for the ballast condition (LC light) for reference purposes.

Table 1. Main parameters of full-scale ship and ship model.

Main Particulars	Symbol	Unit	Full Scale LC Light	Model LC Light	Model LC Medium	Model LC Heavy
Model scale	λ	[-]	-	20	20	20
Length on waterline	L_{WL}	[m]	32.68	1.634	1.662	1.641
Length, overall submerged	L_{OS}	[m]	34.795	1.670	1.740	1.740
Breadth	B	[m]	9.28	0.464	0.464	0.464
Draught	T	[m]	3.30	0.165	0.180	0.195
Displacement volume	∇	[m^3]	599.40	0.075	0.085	0.095
Wetted surface area	S	[m^2]	392.67	0.982	1.058	1.124
Block Coefficient	C_B	[m]	0.60	0.60	0.61	0.64
Midship section coefficient	C_M	[m]	0.86	0.86	0.87	0.89

The three models used for this research are shown in Figures 1–3. The original model is shown in Figure 1, and then two alternatives were tested in order to evaluate their hydrodynamics in calm water. As presented previously, there is not a general rule for ship bulbous bow design. Therefore, the designs shown in Figures 2 and 3 were based on the authors' experience with similar ship designs. It was decided to study inclined and straight bow shapes since the straight bow is common in traditional designs without a bulbous bow, and the vertical bow was considered a limit case of the previous bow shape, which also maximizes the waterline length. For designing these models, the ship lines and all the ship characteristics were kept the same, with the only change being the bulbous that was removed. Then, the bow was closed in two different wavs.

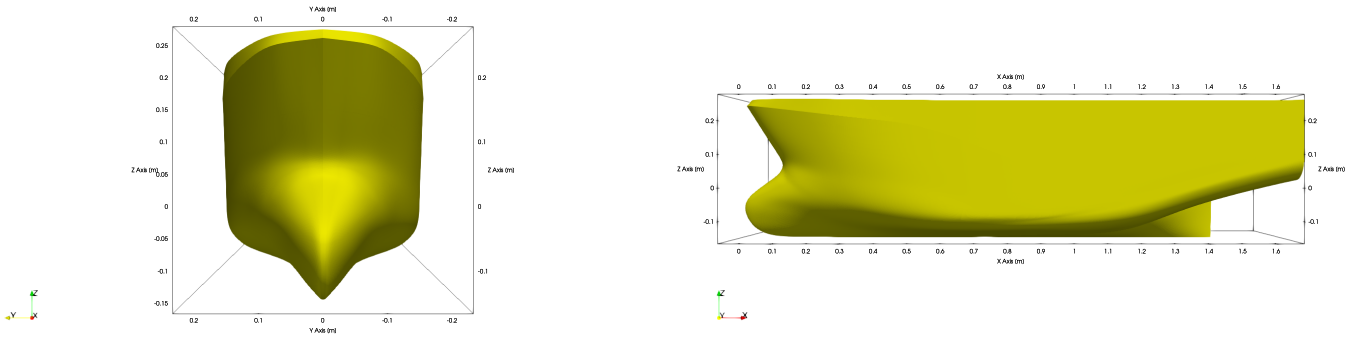

Figure 1. Bulbous bow model (BBM): front view (**left**) and side view (**right**).

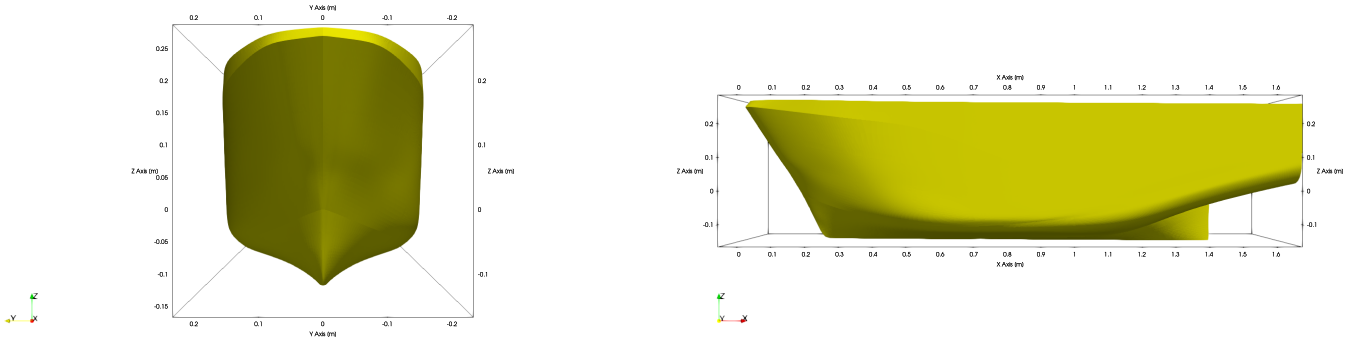

Figure 2. Inclined bow model (IBM): front view (**left**) and side view (**right**).

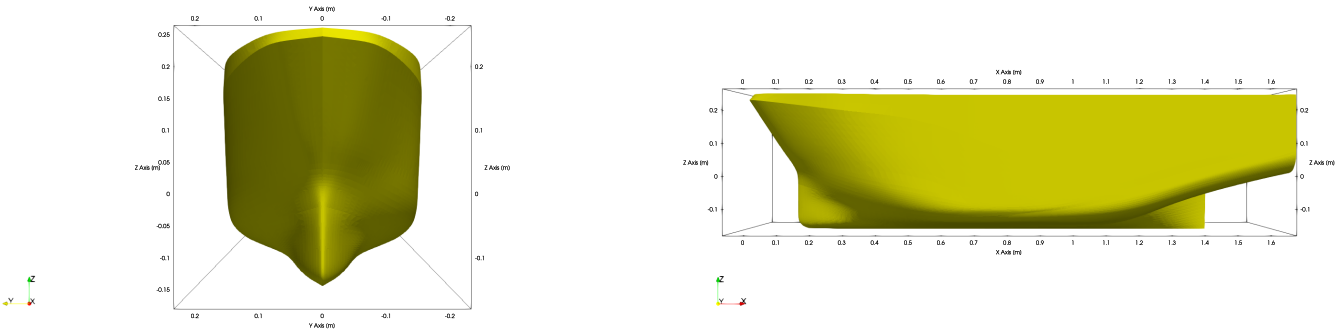

Figure 3. Straight bow model (SBM): front view (**left**) and side view (**right**).

2.2. Experimental Set-Up

The University of Buenos Aires towing tank was used to conduct experimental tests. The tank measures 72 m in length, 3.6 m in width, and has a depth of 2 m. Figure 4 shows a picture of the model. Two trip wires of 1.0 mm were employed to promote turbulence. One is located downstream from the fore perpendicular at a distance equal to five percent of L_{WL}. And another is downstream the bulb fore-end at a distance equal to one-third the bulb length.

The force measurement procedure consists of attaching the ship model, once ballasted, to a dynamometer. An R47 by Kempf & Remmers one-component force transducer capable of handling a full-scale load of ±100 N with a sensitivity of approximately ±1 mV/V was used. The model was only free to move in trim and sinkage.

The resistance measurements' uncertainty analysis considers several components, including hull geometry, towing speed, water temperature, dynamometer calibration, and repeat tests.

The standard uncertainty for each component is estimated individually and then combined using the Root Sum Square (RSS) method [22]. The best estimate of resistance is determined by adopting the mean of repeat resistance measurements. Table 2 shows the uncertainty component of the mean (with N = 4 repeat tests) for four different speeds As seen in Table 2, the dynamometer and the precision of measurement are the major sources of the uncertainties originating in the repeat tests. The expanded uncertainties presented in Table 2 correspond to a 95% confidence level.

Table 2. Combination of uncertainty in measurement for resistance at Fn = 0.14, Fn = 0.26, Fn = 0.37, and Fn = 0.45. Repeat test N = 4.

Uncertainty Components	Fn = 0.14	Fn = 0.26	Fn = 0.37	Fn = 0.45
Hull geometry	0.05	0.05	0.05	0.05
Speed	0.067	0.067	0.067	0.067
Water temp.	0.03	0.03	0.03	0.03
Dynamometer	4.73	1.04	0.35	0.12
Repeat test, Deviation [a]	5.00	3.50	1.50	1.10
Combined for single test	6.88	3.65	1.54	1.11
Repeat test, Deviation of mean	2.50	1.75	0.75	0.55
Combined for repeat mean	5.35	2.04	0.83	0.57
Expanded for repeat mean	10.70	4.08	1.66	1.14

[a] Repeat test, Deviation = (Repeat test, Deviation of mean) × $N^{1/2}$.

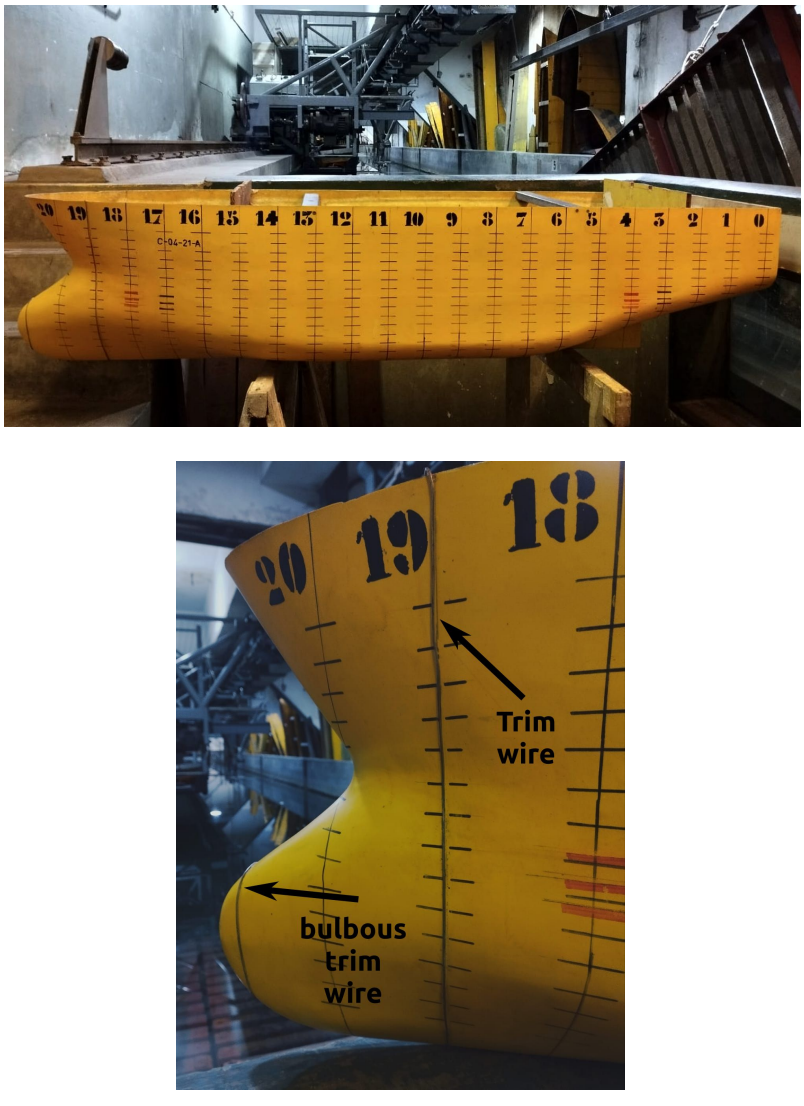

Figure 4. Top: experimental model. **Bottom**: tripwire detail.

3. CFD Description

Nowadays, computational fluid dynamics (CFD) is extended to a wide range of areas. In naval engineering, CFD is used in many topics, with resistance calculation being one of the most interesting ones [8]. OpenFOAM is a commonly used code for this task and in research. This one is an open tool based on the finite volume method that implements the equations for fluid dynamics, Navier–Stokes equations, different numerical schemes,

and turbulence methods, among other equations. In this work, this tool is used for creating the mesh and solving the numerical equations. The software Rhinoceros 7 was used for creating the geometry and Paraview for visualizing the results.

We compared free heave and pitch CFD cases with constrained cases (fixed sinkage and trim) and, even for the highest Fn, we did not find differences of more than 1.5 % in the calculated resistance values. So, although trim and sinkage were monitored in the towing tank tests in this work, we do not compare ship attitudes, because the CFD calculations were carried out with fixed sinkage and trim in order to reduce the computational effort.

3.1. Numerical Equations

When the ship resistance is computed numerically, the equations to be used must imply a Newtonian, turbulent, incompressible, and viscous flow. The equations of the fluid used are then the momentum and mass equations of Navier–Stokes Equations (2) and (3).

$$\nabla \cdot \overline{U_f} = 0 \tag{2}$$

$$\frac{\partial(\rho_f \overline{U_f})}{\partial t} + \nabla(\rho_f \overline{U_f U_f}) = \rho_f g - \nabla p + \mu_f \nabla^2 \overline{U_f} \tag{3}$$

Since the turbulence cannot be solved in all the scales due to the computational resources, a modelization is needed. The Reynolds-Averaged Navier–Stokes (RANS) method is used with the SST k-ω model that provides good results, such as the ones presented in [8]. This model is based on two equations, where k is the turbulent kinetic energy, and ω is the specific dissipation rate.

On the other hand, these kinds of simulations imply the presence of two fluids, air and water. Therefore, an equation that can handle the two fluids is required, that is, the Equation (4) of the Volume of Fluid (VOF) method. This method distinguishes between 0 and 1 for a scalar α, indicating the proportion of fluid contained in the different domain cells.

$$\frac{\partial(\alpha)}{\partial t} + \overline{U_f} \cdot \nabla \alpha = 0 \tag{4}$$

3.2. Numerical Domain

A 3D domain was selected with the dimensions presented in Figure 5 after conducting some simulations verifying that no blockage effect was present. Therefore, the different domain walls are chosen far enough from the model to avoid any effect produced by those walls.

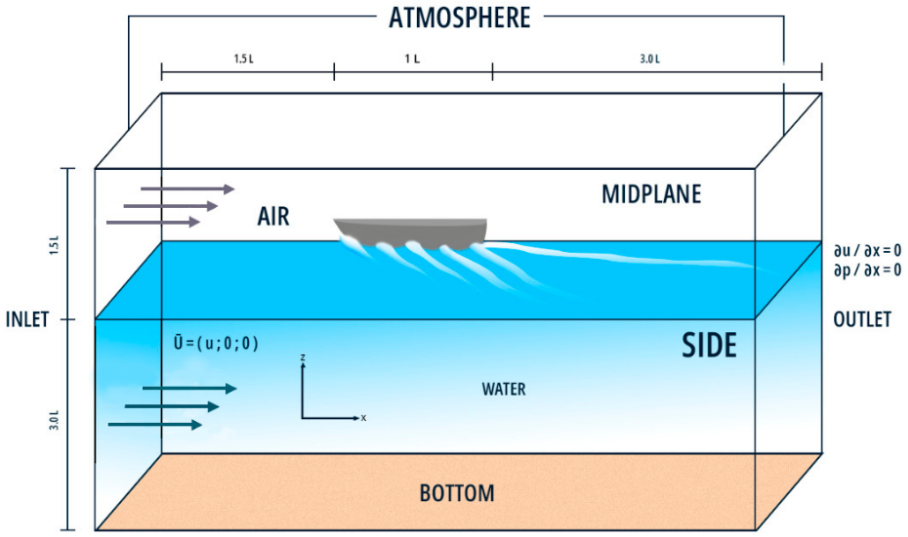

Figure 5. Problem domain.

3.3. Numerical Boundary Conditions

The numerical boundary conditions are presented in Table 3. It should be noted that only half of the ship is computed in order to optimize computational resources. This implies the use of the *symmetry* boundary condition.

Table 3. Numerical boundary conditions.

Patch	U	p	k	ω	μ Turbulent
Inlet	uniform	fixed flux	fixed value	fixed value	fixed value
Outlet	zero gradient	zero gradient	zero gradient	zero gradient	zero gradient
Atmosphere	zero gradient	zero gradient	zero gradient	zero gradient	zero gradient
Bottom	symmetry	symmetry	symmetry	symmetry	symmetry
Midpl/Side	symmetry	symmetry	symmetry	symmetry	symmetry
Ship	no slip	fixed flux	wall function	wall function	wall function

3.4. Numerical Mesh

The mesh used for the numerical analysis was created using blockMesh and snappyHexMesh, both of these tools are provided by OpenFOAM. The mesh is structured with 92% hexahedrons and divided into uniform and graded zones. Figures 6 and 7 present the final mesh, which has a horizontal expansion ratio of 1.3 and 1.2 in the 'x' and 'y' axes, respectively, and a vertical expansion ratio of 1.2, all towards the center zone. The vessel is contained within a block composed of hexahedrons with an aspect ratio of one, except for the interface zone, where the cells were reduced by 25% of their height to accurately capture wave height. The mesh is designed to ensure that the y+ value remains below 5 in all cases.

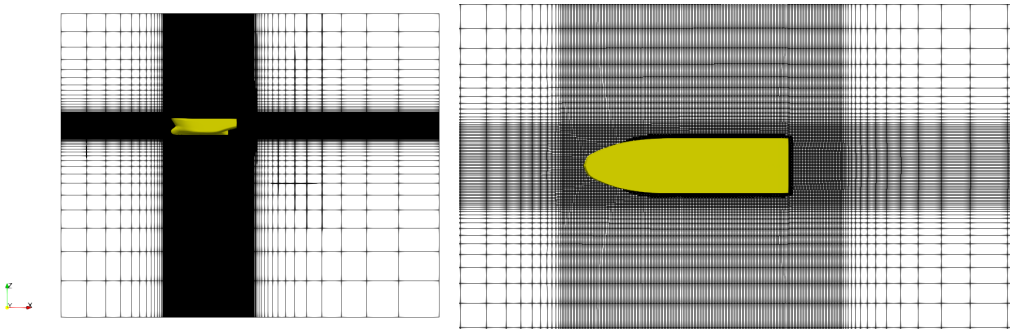

Figure 6. General mesh view. Mesh 4.

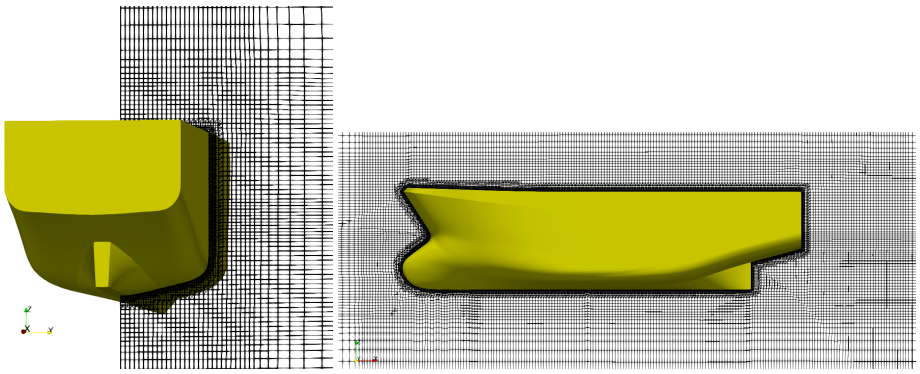

Figure 7. Mesh zoom for different orientations. Mesh 4.

A mesh validation was conducted in order to see that the results provided by the numerical procedure were obtained with a minimum error. Therefore, a convergence study was conducted using the heavy LC and Fn 0.45. The different meshes tested, with the cell size in the center box refined systematically by a ratio of 1.2, presented an oscillatory

convergence, shown in Table 4. All the meshes presented show an error that might be acceptable since it is lower than 4%. Finally, the simulations were conducted using a first-order pseudotransient time scheme that employs a specific local time step. Therefore, there is no need for further numerical sensitivity analysis. The numerical set-up is validated.

Table 4. Mesh validation.

Case	Mesh Cells	Fn	F [N]	Error (%)
EFD	-	0.45	40.27	-
Mesh 1	633.938	0.45	40.26	0.02
Mesh 2	903.744	0.45	41.76	3.70
Mesh 3	1.213.419	0.45	40.34	0.17
Mesh 4	2.485166	0.45	41.16	2.21

4. Results

4.1. CFD Validation

Before analyzing the differences between the use of the bulbous bow and the two different cases without a bow, the comparison between CFD and EFD drag resistance for the case with bulbous was performed. Therefore, the drag forces obtained for the case with bulbous bow at different speeds and different load conditions were compared. In Figure 8, the drag forces are presented in a dimensionless way using the coefficient C_T, which is defined as

$$C_T = \frac{Drag}{\frac{1}{2}\rho S v^2} \tag{5}$$

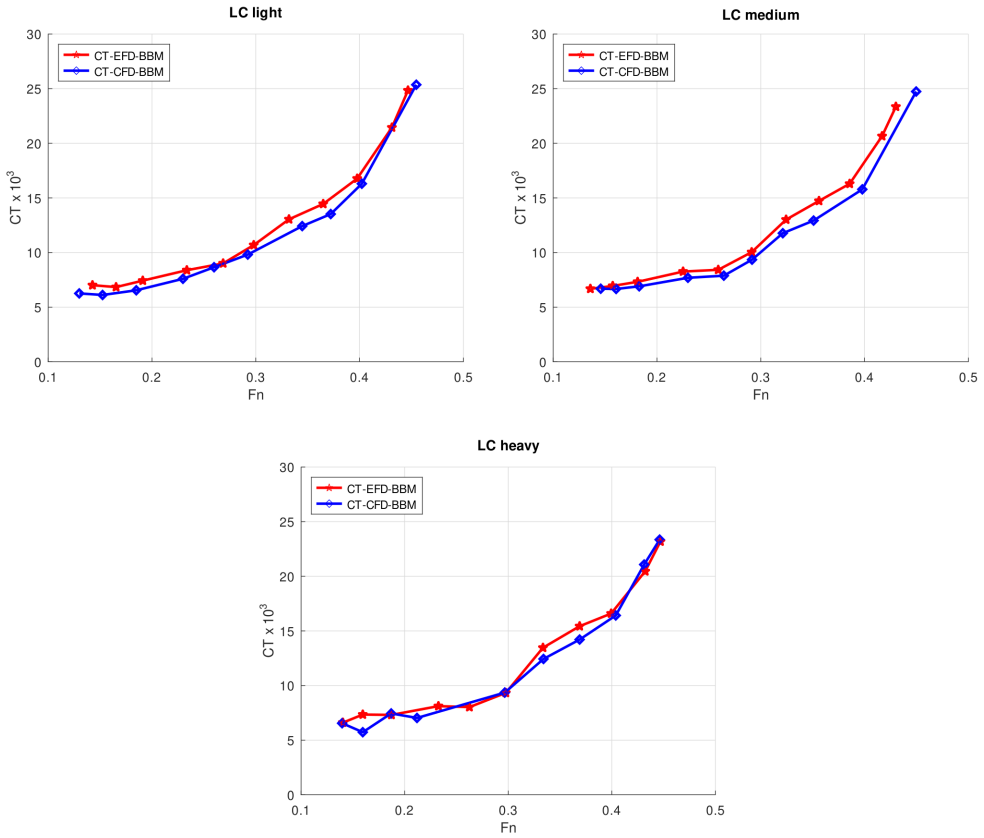

Figure 8. C_T vs Fn for LC light, LC medium, and LC heavy.

The numerical results present a good agreement with the experimental ones for all the speeds and load conditions. In addition, the wave pattern generated by the ship model is also compared in Figure 9, showing an apparently similar wake. According to these results, the numerical procedure for the wake evaluation and the drag forces estimation can be validated.

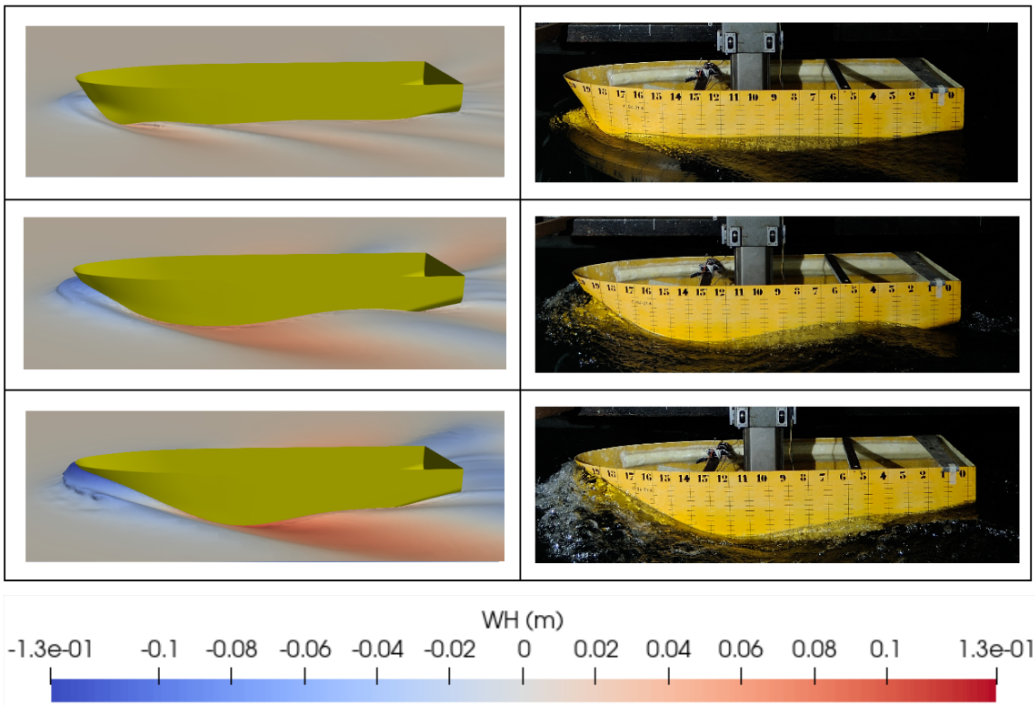

Figure 9. Wave pattern for different Fn and draught = LC heavy. Left: CFD. Right: EFD. First row: Fn = 0.26, second row: Fn = 0.37, third row: Fn = 0.45.

The evaluation of different drafts is because fishing ships sail under different situations depending on their activities and load. For instance, when the ship is fishing, it leaves the port with an empty load, and when it is coming back to port it has fish inside it. Also, the speed is determined by the sea conditions, weather, fishing restrictions, etc. In this work, the selected ship is designed for an operation of Fn 0.35. Lower velocities will be used in port and other fishing activities or even when that speed is unreachable due to weather conditions. The results presented in Figures 8 and 9 show the typical behavior of these kinds of hull ships. For Fn < 0.3, the major component of the resistance is the viscous resistance growing C_T linearly. This speed is the critical speed, since for higher velocities, the C_T increases in a exponential way. The main reason for this behavior is that at low speeds, the wave resistance has almost no influence on the total resistance, while becoming predominant at higher speeds.

Once the CFD has been validated, its use makes it possible to obtain data that are difficult or very complicated to measure experimentally, for instance, the pressure distribution around the hull. In Figure 10, the dimensionless pressure C_P around the hull for the BBM case is shown. This dimensionless parameter is defined as follows:

$$C_P = \frac{p - p_\infty}{\frac{1}{2}\rho_\infty V_\infty^2} \tag{6}$$

where $p - p_\infty$ is the dynamic pressure.

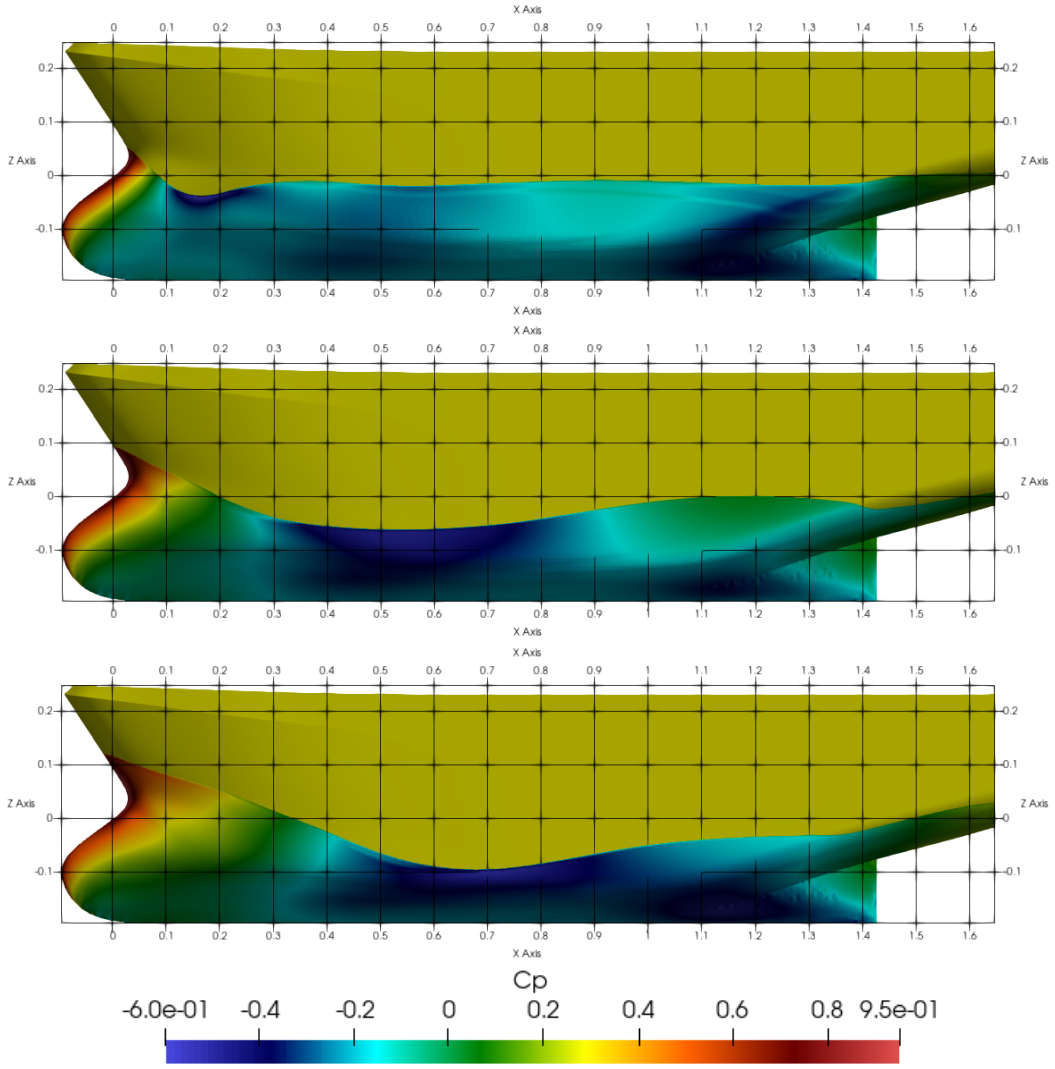

Figure 10. Cp distribution for Fn = 0.26, Fn = 0.37, and Fn = 0.45, T = LC Heavy.

When studying wave generation, it is essential to consider the distribution of pressure over the hull. The pressure distribution over the hull indicates the size and shape of the waves. In addition, this pressure distribution may provide insight into the distribution of forces around the hull, highlighting areas that are more susceptible to higher forces. In Figures 10–12, different pressure zones are presented for the three cases of study. It is noticeable that these contours are presented for different Fn numbers and load conditions. The pressure distribution and wave formation change with the Fn number, as shown in Figure 10 for the bulbous bow case where the wake formation is bigger for higher Fn numbers. Additionally, the maximum pressure distribution expands to a larger area as Fn increases. Figures 11 and 12 show that hulls without a bulbous bow have a very similar pressure distribution and wake formation. In contrast, hulls with a bulbous bow have a more linear wake formation and do not present a hollow in the shoulders of the ship, as is the case with hulls without a bulbous bow.

Based on these contours, it can be concluded that for optimal efficiency and reduced drag, a smooth pressure distribution over the hull is necessary. An even pressure distribution reduces disturbances in the water, resulting in less energy loss due to wave generation and therefore less resistance. Conversely, an uneven pressure distribution may produce significant disturbances in the water, resulting in more waves and greater resistance. The distributions are highly dependent on various factors, and the behavior changes once the bulbous bow is introduced.

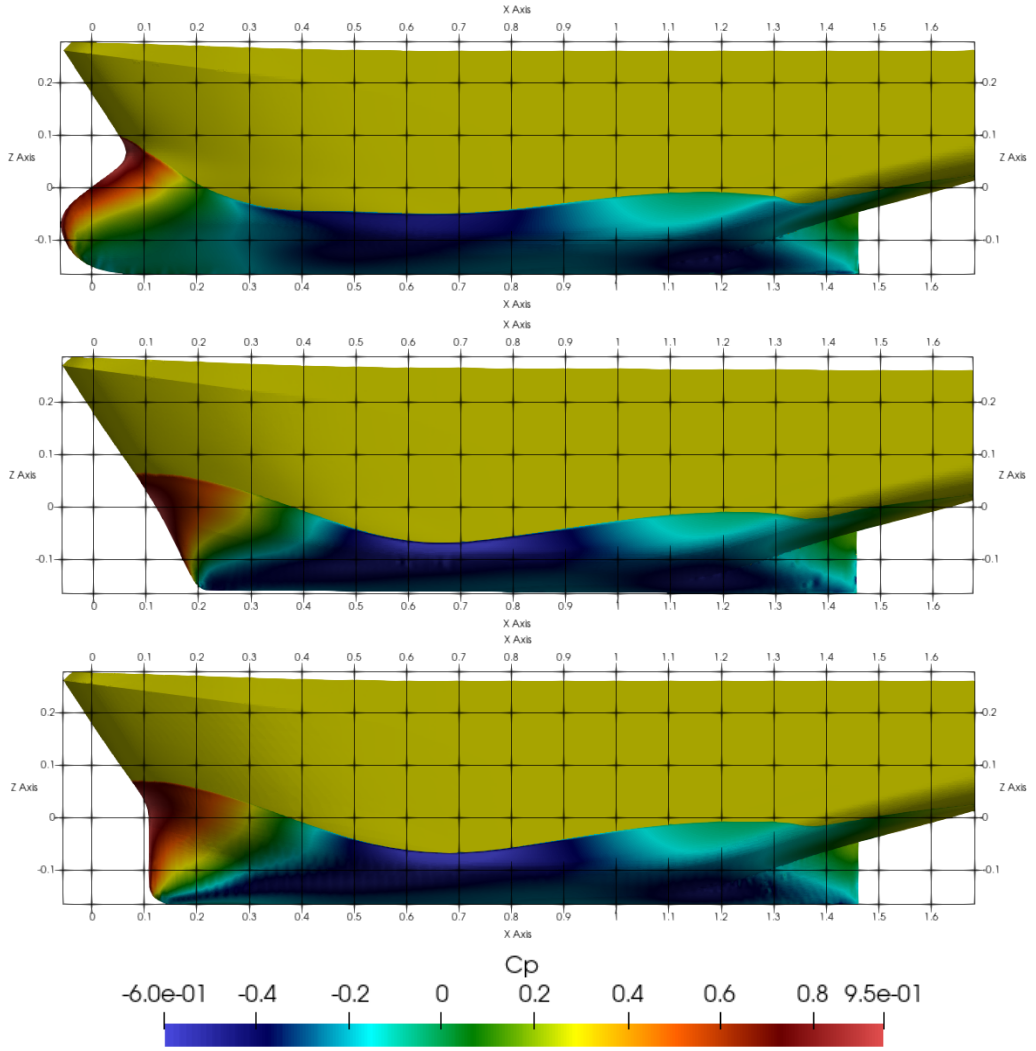

Figure 11. Cp distribution for the different bulbous bows for Fn = 0.37, T = LC light.

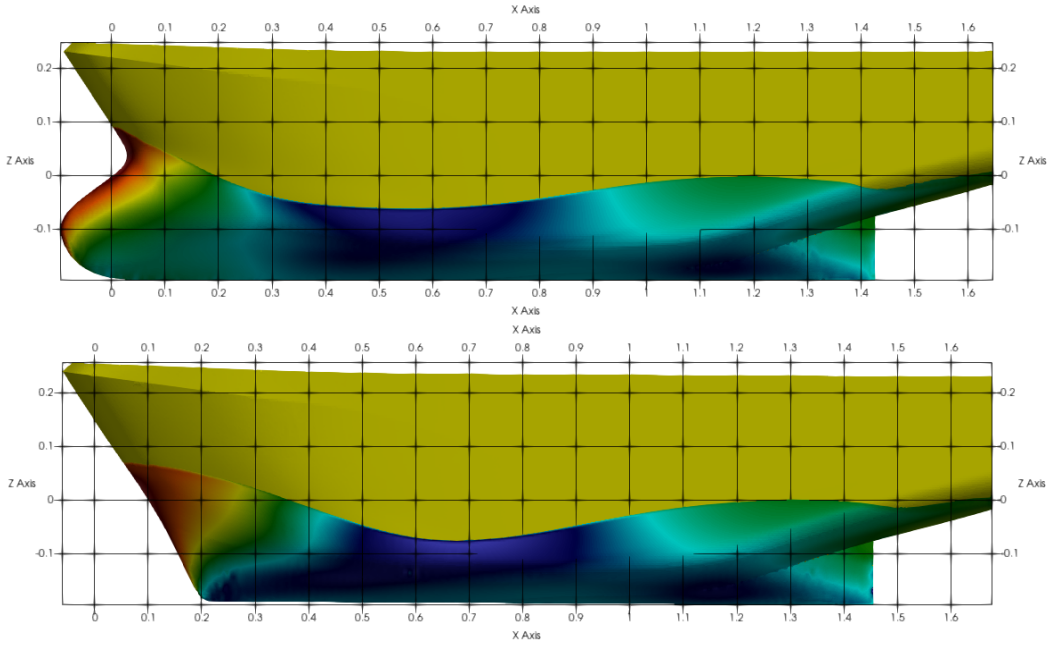

Figure 12. *Cont.*

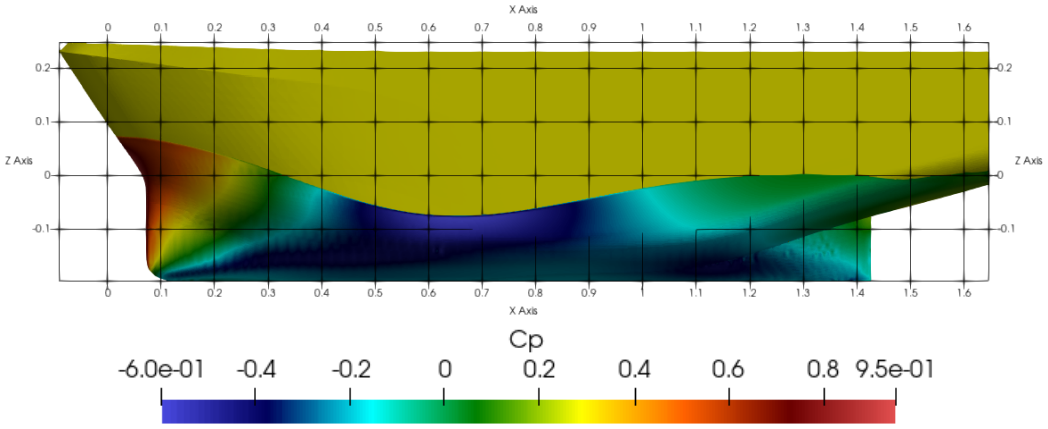

Figure 12. Cp distribution for the different bulbous bows for Fn = 0.37, T = LC heavy.

As fishing vessels operate at a wide range of speeds and loads, i.e., when fishing, leaving port, or returning from the ground with fish, the hull shape and resistance calculation should be carefully evaluated, as one hull shape may work for one load condition and speed range but not for the rest. In this situation, it must be the ship owner who decides the optimum range of operation.

4.2. Bows Designs Analysis

After evaluating the ship model resistance numerically and experimentally for the case with a bulbous bow, the model is redesigned removing the bulbous bow. Two different configurations for this kind of vessel will be implemented and evaluated. Those cases will bring more details about the hydrodynamic behavior, providing valuable information for this kind of ship with limited research. The evaluation between the two new designs without bulbous bows and the original one with bulbous bows will be performed only numerically, keeping the same mesh, range of velocities, and load conditions. In order to better appreciate the results and the differences between hulls, the resistance will be split in two, for moderate speeds, Fn $<$ 0.3 in Figure 13, and for higher speeds, Fn $>$ 0.3 in Figure 14.

In Figure 13 and for Fn $<$ 0.3, we can appreciate that there is not a clear tendency or any hull that works better for the three loads conditions at this range of speed. For LC light, the hull BBM produces less drag until Fn 0.15. From this speed, there is a linear growth of resistance, and it is the worst hull in terms of resistance for Fn between 0.2 and 0.25. For this LC, the hull SBM always offers less resistance than the IBM hull. Indeed, it is the most efficient hull for the range of speed 0.2–0.25. The IBM model seems to be the less efficient hull for all the range of speed.

When LC medium is evaluated, in Figure 13, we can appreciate that the hull BBM is less efficient for velocities lower than Fn $<$ 0.25. On the contrary, and in comparison with the LC light, the IBM hull is the most efficient. However, this hull seems to be efficient for a speed lower than Fn $<$ 0.25, since from this velocity onwards, the resistance grows exponentially and it becomes larger than the BBM case.

For the LC heavy, there is not a clear tendency that allows one to determine which hull is better. Only when the speed is higher than 0.25, the BBM becomes a more efficient hull. For the different load conditions and hull shapes, we can appreciate that Fn 0.25 is a critical value where the ship resistance curve behavior changes.

In Figure 14, we analyze the resistance produced by the three hulls for higher speeds. In this range of speeds, the wave resistance is the most relevant part of the total resistance. For the three load conditions, we can appreciate an exponential growth in the total resistance for all of the hulls. For the three load conditions, the hull BBM performs better for the whole range of speed. The IBM and the SBM have almost identical drag for the load conditions of medium and heavy. For the LC light, the SBM hull has less drag than the IBM for Froude

numbers lower than 0.4, demonstrating almost the same for higher speeds. It is remarkable that for Fn $>$ 0.35, the increment of resistance makes the bulbous bow the best.

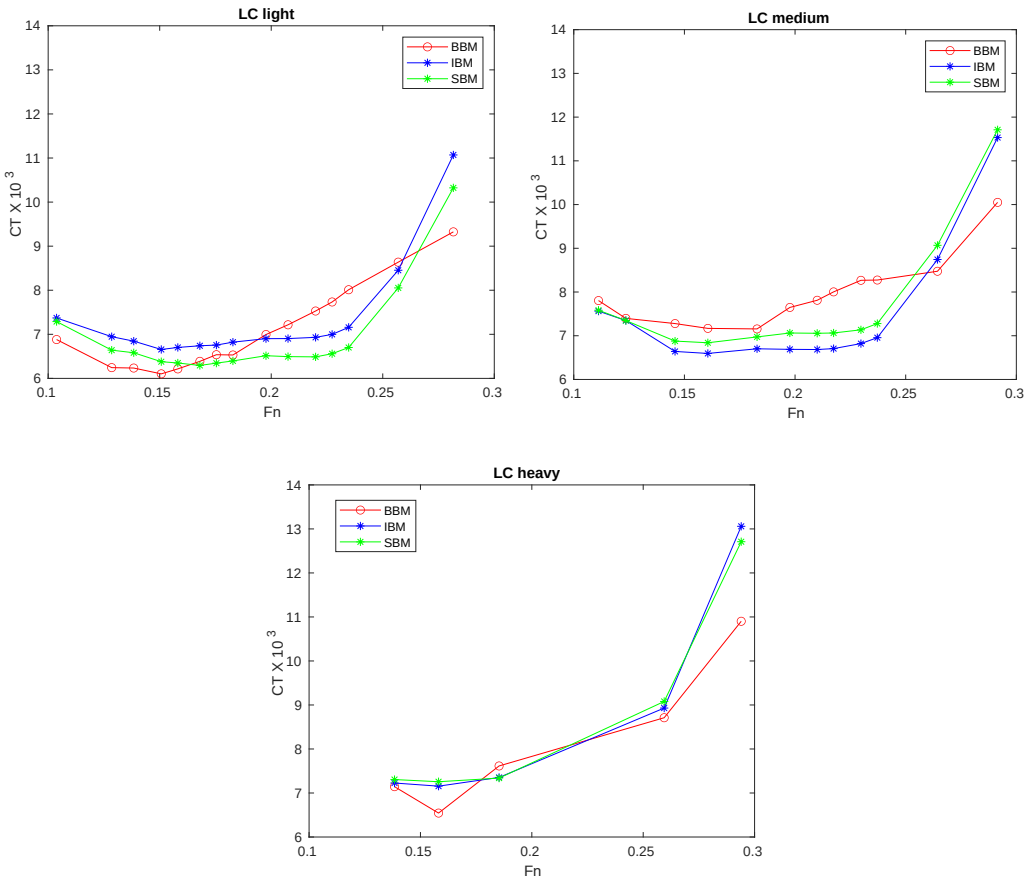

Figure 13. C_T vs. Fn comparison for the three hulls and for Fn $<$ 0.3.

Based on the previous results, it is clear that the ship owner must decide the ship shape based on the speed and load condition that is more frequently used. However, the ship with a bulbous bow seems to be the best option at least for calm water. From the numerical results, we can also obtain a force decomposition, in viscous and pressure force, that will indicate the dominance of one or other forces for each velocity. This will help in the design process because it will clearly identify the area for shape optimization.

For instance, Figure 15 presents the total force decomposed in viscous (FV) and pressure (FP) force for LC light and the original BBM ship model. From this graph, we can appreciate that the viscous resistance grows linear, dominating for Fn $<$ 0.25. On the other side, pressure resistance grows linear until Fn = 0.25. From this point, the pressure resistance becomes dominant, and it grows almost exponentially. It is clear then that for this ship, the critical point, as mentioned before, is Fn = 0.25. From this point onwards, the pressure resistance that is related to wave making plays a significant role.

Figure 16 presents the viscous force for the three hulls and the three load conditions. From these results, we can conclude that the viscous forces grow linear for all the cases. The BBM model is expected to have a higher viscous resistance due to its larger wetted surface area. This effect may be slightly noticeable for Fn values greater than 0.25. For lower Fn values, the forces are too small to draw any conclusions.

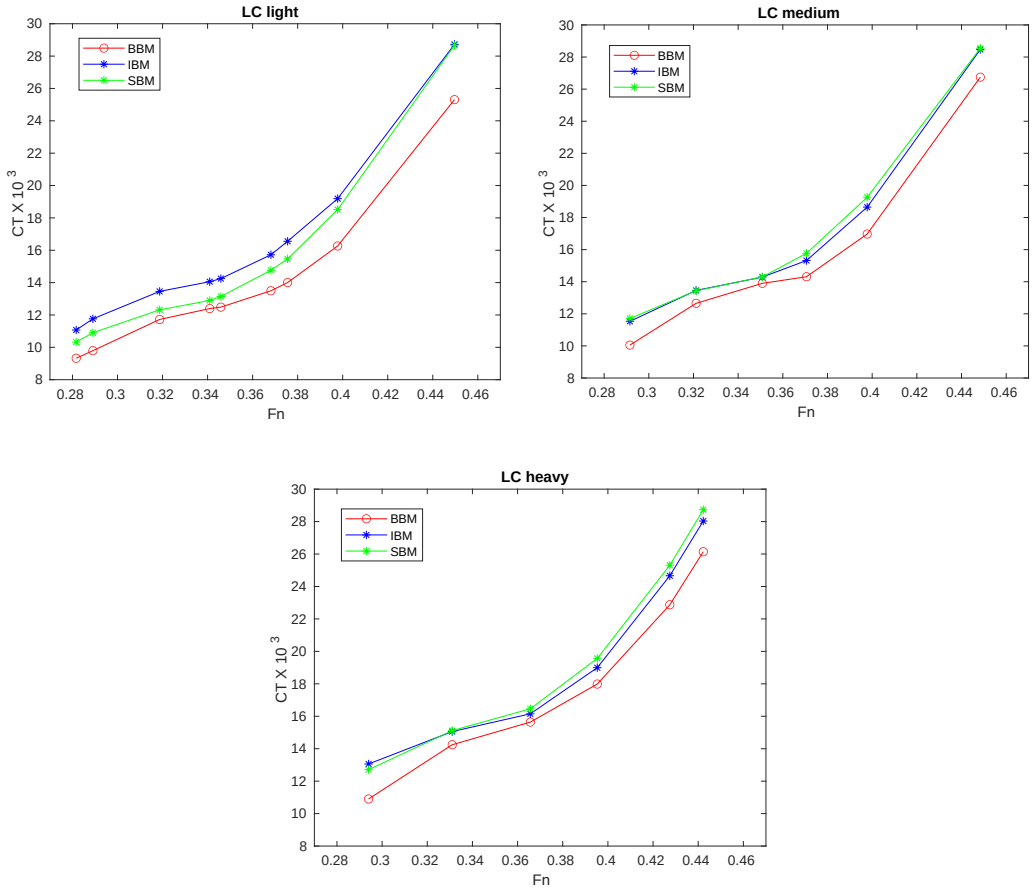

Figure 14. C_T vs. Fn comparison for the three hulls and for Fn $>$ 0.3.

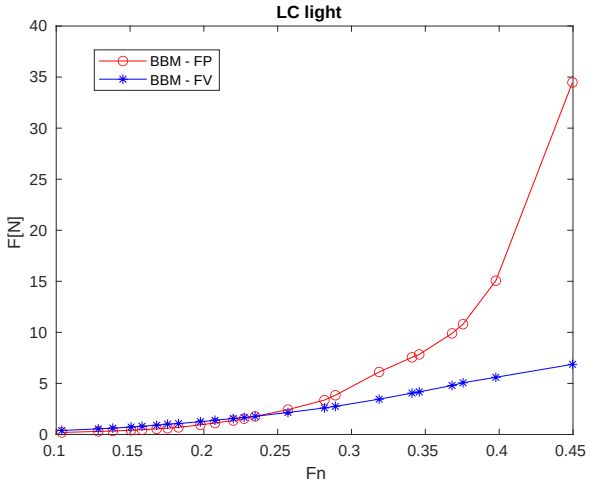

Figure 15. Pressure (FP) and viscous (FV) force for LC light and BBM.

Figure 17 presents the pressure forces for the three load conditions and ship hulls. The behavior of this force is similar for the different conditions. There is a linear growth until Fn = 0.25. Before this point, the pressure resistance was relatively low in comparison with the produced for higher Fn numbers. From Fn = 0.25 onwards, the growth in pressure resistance is almost exponential, becoming part of the resistance and the dominant one when compared with Figure 16. Besides, we can appreciate that the difference in total resistance between hulls is mainly due to the pressure resistance.

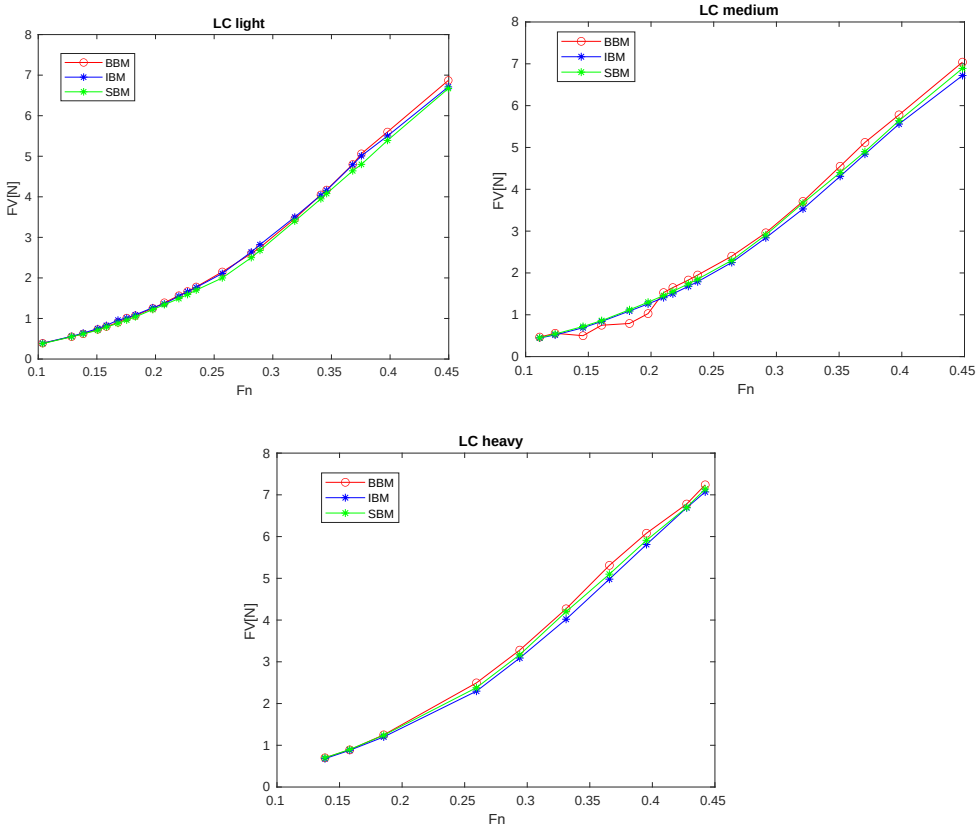

Figure 16. Viscous force comparison for the three hulls.

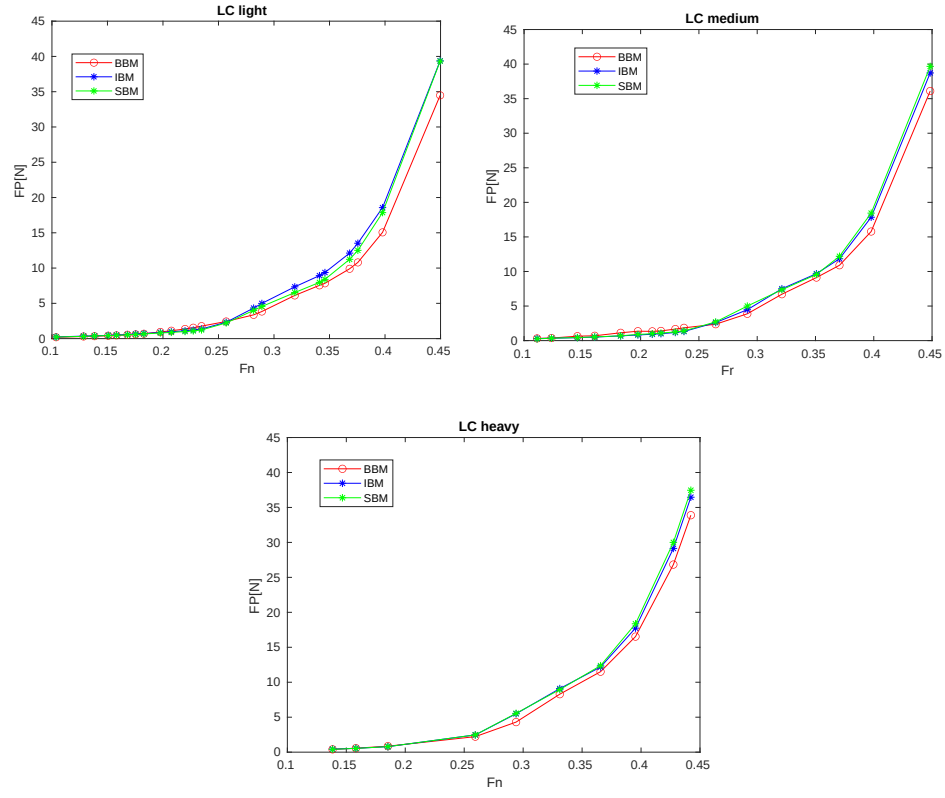

Figure 17. Pressure force comparison for the three hulls.

5. Conclusions

The conducted research tries to give more details about the hydrodynamic influence of three different bow configurations in fishing vessels. These configurations are the typical ones that can be found in this type of vessel. The presented studies were conducted at the model scale, either experimentally or numerically. The main conclusions are as follows:

- There is a critical point at Fn = 0.25 from where the resistance grows exponentially due to the high influence of the pressure resistance that is linked with wave resistance.
- For low velocities, the hulls with no bulbous bow in general show good efficiency until Fn 0.25, from where the hulls do not seem to have the correct shape.
- For the different load conditions and speeds after Fn = 0.25, the case of BBM shows higher efficiency. It is clear then that the bulbous bow works better, reducing pressure resistance.
- The viscous resistance grows linearly for all the cases. This resistance becomes more significant in the total resistance for Fn $<$ 0.25, although the BBM does not seem to change the total amount of viscous force that much.
- The pressure resistance is predominant from Fn 0.25 onwards. This resistance is the main source of resistance, which means ship designers should focus on reducing this component of resistance.
- The pressure distribution around the hull demonstrates how it changes with the Fn number, revealing a larger hollow wake as Fn increases.
- The pressure distribution is practically the same for the two cases without a bulbous bow. When compared with a bulbous bow hull, it is noticeable that the hollows in the ship's shoulders are less pronounced, sometimes resulting in a nearly linear wake generation around the hull.

Finally, this research brings new information that is the first step to fully understanding the hydrodynamics of these kinds of ships and their design. Future research should focus on sailing in waves, which will guide us to decide if the conclusions for calm water are also supported in waves.

Author Contributions: Validation, S.O., R.S. and A.D.O.; Formal analysis, F.P.A.; Investigation, H.R.D.O. and F.P.A. All authors have read and agreed to the published version of the manuscript.

Funding: The Ministry of Science, Technology and Innovation of the Argentine Republic (MINCyT—Proyecto de Investigación y Desarrollo Tecnológico de la Iniciativa Pampa Azul—B2), the Universidad de Buenos Aires, Facultad de Ingeniería (Grant Peruilh).

Data Availability Statement: Data are contained within the article.

Acknowledgments: This work was supported by the Spanish Ministry of Ciencia e Innovación through grant PID2022-140481OB-I00. We thank the Argentine shipyard TecnoPesca Argentina for providing the fishing vessel lines.

Conflicts of Interest: The authors declare no conflicts of interest.

Nomenclature

List of variables:

L	Ship total length (m)
L_{WL}	Ship waterline length (m)
B	Ship beam (m)
T	Ship draught (m)
∇	Volumetric displacement of ship (m^3)
S	Wetted surface area (m^2)
C_B	Block coefficient
λ	Scale
C_M	Midship section coefficient
Fn	Froude number (Fn = $V\sqrt{gL_{WL}}$)

g	gravitational constant (m/s^2)
F	Total drag resistance (N)
FV	Viscous resistance (N)
FP	Pressure resistance (N)
ρ_∞	Water density
C_P	Pressure coefficient
C_T	Drag force coefficient coefficient
WH	Wave height (m)

References

1. Guldhammer, H.E.; Harvald, S. *SHIP RESISTANCE—Effect of Form and Principal Dimensions*; Danish Technical Press: Copenhagen, Danmark, 1965.
2. Holtrop, J. A statistical re-analysis of resistance and propulsion data. *Int. Shipbuild. Prog.* **1984**, *31*, 272–276.
3. Bilec, M.; Obreja, C.D. Ship resistance and powering prediction of a fishing vessel. *IOP Conf. Ser. Mater. Sci. Eng.* **2020**, *916*, 012011. [CrossRef]
4. Matínez-López, A.; Díaz Ojeda, H.R.; Míguez González, M.; Marrero, Á. Environmental Inefficiencies of Short Sea Shipping Vessels by Optimization Processes Based on Resistance Prediction Methods. *J. Mar. Sci. Eng.* **2022**, *10*, 1457. [CrossRef]
5. Larsson, L.; Raven, H.; Paulling, J. *Ship Resistance and Flow*; Principles of Naval Architecture; Society of Naval Architects and Marine Engineers: Alexandria, VR, USA, 2010.
6. Ferreiro, L.D. The social history of the bulbous bow. *Technol. Cult.* **2011**, *52*, 335–359. [CrossRef]
7. Barrass, B. *Ship Design and Performance for Masters and Mates*; Elsevier: Amsterdam, The Netherlands, 2004.
8. Díaz-Ojeda, H.; Pérez-Arribas, F.; Turnock, S.R. The influence of dihedral bulbous bows on the resistance of small fishing vessels: A numerical study. *Ocean. Eng.* **2023**, *281*, 114661. [CrossRef]
9. Pérez-Arribas, F.; Silva-Campillo, A.; Díaz-Ojeda, H.R. Design of Dihedral Bows: A New Type of Developable Added Bulbous Bows—Experimental Results. *J. Mar. Sci. Eng.* **2022**, *10*, 1691. [CrossRef]
10. Ren, Z.; Wang, J.; Wan, D. Numerical Simulations of Ship Bow and Shoulder Wave Breaking in Different Advancing Speeds. In Proceedings of the International Conference on Offshore Mechanics and Arctic Engineering, Madrid, Spain, 17–22 June 2018; American Society of Mechanical Engineers: New York City, NY, USA, 2018; p. V07AT06A010. [CrossRef]
11. Chakraborty, S. What's Importance of Bulbous Bow of Ships. *Marine Insight*. 21 May 2017. Available online: https://www.marineinsight.com/naval-architecture/why-do-ships-have-bulbous-bow/ (accessed on 1 February 2024).
12. Kracht, A. Design of bulbous bows. In Proceedings of the SNAME Annual Meeting, New York, NY, USA, 16–18 November 1978; Volume 86.
13. Hoyle, J.W.; Cheng, B.H.; Hays, B. *A Bulbous Bow Design Methodology for High-Speed Ships*; Society of Naval Architects and Marine Engineers-Transactions; Society of Naval Architects and Marine Engineers: Alexandria, VR, USA, 1986; Volume 94.
14. Hagen, G.E.A. *A Guide for Integrating Bow Bulb Selection and Design into the U.S. Navy's Surface Ship Hull Form Development Process, Naval Sea Systems Command*; Technical Note No. 885-55W-TN0001; NAVSEA: Washington, DC, USA, 1983.
15. Peri, D.; Rossetti, M.; Campana, E.F. Design optimization of ship hulls via CFD techniques. *J. Ship Res.* **2001**, *45*, 140–149. [CrossRef]
16. Sharma, R.; Sha, O.P. Practical hydrodynamic design of bulbous bows for ships. *Nav. Eng. J.* **2005**, *117*, 57–76. [CrossRef]
17. Watle, A. Flexible Bulbous Bow Design-A Hydrodynamic Study. Master's Thesis, NTNU, Trondheim, Norway, 2017.
18. Bertolotti, M.; Verazay, G.; Pagani, A.; Errazti, E.; Buono, J. Flota pesquera Argentina. Evolucion 1960–1998 con una actualizacion al 2000. In *El Mar Argentino y Sus Recursos Pesqueros. Evolución de la Flota Pesquera, Artes de Pesca y Dispositivos Selectivos*; INIDEP: Mar del Plata, Argentina, 2001.
19. Oyuela, S.; Sosa, R.; Otero, A.D.; Arribas, F.P.; Diaz-Ojeda, H.R. An experimental and numerical hydrodynamic study on the Argentinian fishing vessels. *IOP Conf. Ser. Mater. Sci. Eng.* **2023**, *1288*, 012047. [CrossRef]
20. Arribas, F.P.; Oyuela, S.; Otero, A.D.; Sosa, R.; Diaz-Ojeda, H.R. The use of Ctrl+Z in ship design: Removing a bulbous bow. *IOP Conf. Ser. Mater. Sci. Eng.* **2023**, *1288*, 012044. [CrossRef]
21. Specialist Committee: Procedures for Resistance, Propulsion and Propeller Open Water Tests of 23rd ITTC 2002. *ITTC—Recommended Procedures and Guidelines: Model Manufacture, Ship Models*; ITTC: Nairobi, Kenya, 2002
22. 28th ITTC Quality Systems Group. *ITTC—General Guidelines for Uncertainty Analisys in Resistance Tests*; ITTC: Nairobi, Kenya, 2017.